



CHORUS

This is the accepted manuscript made available via CHORUS. The article has been published as:

Anisotropic magnetotransport and exotic longitudinal linear magnetoresistance in WTe_2 crystals

Yanfei Zhao, Haiwen Liu, Jiaqiang Yan, Wei An, Jun Liu, Xi Zhang, Huichao Wang, Yi Liu, Hua Jiang, Qing Li, Yong Wang, Xin-Zheng Li, David Mandrus, X. C. Xie, Minghu Pan, and Jian Wang

Phys. Rev. B **92**, 041104 — Published 6 July 2015

DOI: [10.1103/PhysRevB.92.041104](https://doi.org/10.1103/PhysRevB.92.041104)

Anisotropic Magnetotransport and Exotic Longitudinal Linear Magnetoresistance in WTe₂ Crystals

Yanfei Zhao^{1,2}, Haiwen Liu^{1,2}, Jiaqiang Yan^{3,4}, Wei An^{2,5}, Jun Liu⁶, Xi Zhang^{1,2}, Huichao Wang^{1,2}, Yi Liu^{1,2}, Hua Jiang⁷, Qing Li⁸, Yong Wang⁶, Xin-Zheng Li^{2,5}, David Mandrus^{3,4}, X. C. Xie^{1,2}, Minghu Pan^{9,*} and Jian Wang^{1,2*}

¹ International Center for Quantum Materials, School of Physics, Peking University, Beijing 100871, China

² Collaborative Innovation Center of Quantum Matter, Beijing 100871, China

³ Department of Materials Science and Engineering, University of Tennessee, Knoxville, Tennessee 37996, USA.

⁴ Materials Science and Technology Division, Oak Ridge National Laboratory, Oak Ridge, Tennessee 37831, USA.

⁵ School of Physics, Peking University, Beijing 100871, China

⁶ Center of Electron Microscopy, State Key Laboratory of Silicon Materials, Department of Materials Science and Engineering, Zhejiang University, Hangzhou, 310027, China

⁷ College of Physics, Optoelectronics and Energy, Soochow University, Suzhou 215006, China

⁸ Institute of Functional Nano and Soft Materials (FUNSOM) and Collaborative Innovation Center of Suzhou Science and Technology, Soochow University, Jiangsu 215123, China.

⁹ School of Physics, Huazhong University of Science and Technology, Wuhan 430074, China.

*Correspondence and requests for materials should be addressed to J. W. (email: jianwangphysics@pku.edu.cn) or to M. P. (email: mhupan@gmail.com)

WTe₂ semimetal, as a typical layered transition-metal dichalcogenide, has recently attracted much attention due to the extremely large, non-saturating parabolic magnetoresistance in perpendicular field. Here, we report a systematic study of the angular dependence of the magnetoresistance in WTe₂ single crystal. The significant anisotropic magnetotransport behavior in different magnetic field directions and violation of the Kohler's rule are observed. Unexpectedly, when the applied field and excitation current are both parallel to the tungsten chains of WTe₂, an exotic large longitudinal linear magnetoresistance as high as 1200% at 15 T and 2 K is identified. Our results imply that, WTe₂ semimetal due to its balanced hole and electron populations seems to be the first material reported that large longitudinal linear magnetoresistance appears when the external magnetic field is parallel to the applied current. Our work will stimulate studies of the

double-carrier correlated materials and corresponding quantum physics.

PACS number: 72.15.Eb, 72.15.Gd, 72.80.Ga, 75.47.-m

In contrast to the classical quadratic magnetoresistance (MR) in metals and semiconductors, linear magnetoresistance (LMR) is an unusual phenomenon in condensed matters. LMR has been found only in limited materials, including silver chalcogenides [1], multilayer epitaxial graphene [2], topological insulators [3-5], three dimensional Dirac semimetal such as Cd_3As_2 [6-8] and TlBiSSe [9], which has often been interpreted by either the theory proposed by Abrikosov [10] or the inhomogeneity in materials [1]. LMR behaviors are usually observed in a magnetic field applied perpendicular to the direction of the excitation current and have become one of the significant research interests in condensed matter physics and material science.

Semimetal tungsten ditelluride (WTe_2), due to its extremely large, non-saturating magnetoresistance has attracted significant research interest recently [11-17]. WTe_2 is a typical layered transition-metal dichalcogenide (TMD) with tungsten chains sandwiched by adjacent chalcogenide layers. The extremely small overlap between the bottom of conduction band and the top of valance band in WTe_2 results in many interesting properties, such as the complicated band structure with multiple Fermi pockets [11, 12], the XMR effect reaching $1.3 \times 10^7\%$ at 60 T and 0.53 K in perpendicular field [11], the pressure induced superconductivity [15, 16], and the predicted potential topological property [17]. However, detailed angle-dependent MR study, representing anisotropic properties of WTe_2 , has not been fully investigated and still remains unclear.

In this paper, we report a systematic study to reveal the anisotropic transport behavior in WTe_2 single crystal. A large residual resistance ratio (RRR) of 741 in zero-field and a significant anisotropic resistivity as well as the anisotropic magnetotransport behavior in different magnetic field directions are observed. Strikingly, when the applied magnetic field is parallel to excitation current along the tungsten chains (a axis) of WTe_2 , an exotic large longitudinal LMR as high as 1200% at 15 T and 2 K is identified. Our results suggest that, due to its balanced hole and electron populations, WTe_2 may be the first material reported for that the longitudinal LMR appears when the magnetic field is applied parallel to the applied current.

W and Te shots in an atomic ratio of 1:49 were placed in a 5 ml Al₂O₃ crucible to grow the WTe₂ single crystals. A catch crucible containing quartz wool was mounted on top of growth crucible and both were sealed in a silica ampoule under approximately 1/3 atmosphere of high pure argon gas. The sealed ampoule was heated up initially to 1100°C and kept for 6 hours, then cooled down to 500°C over 96 hours. The Te flux was separated from single crystals by using a centrifuge once the temperature reaches 500°C. The WTe₂ single crystal grown by this method, further studied by FEI Tecnai F20 transmission electron microscope operated at 200 kV, is proven to be of high quality. Figure 1(a) displays the atomically high-resolution transmission electron microscopy (HRTEM) image, suggesting the crystal growth preferentially along the [001] direction (*c* axis). Figure 1(b) shows the selected area electron diffraction (SAED) pattern looking down the [100] zone, further indicating the single crystal structure of WTe₂. Both HRTEM image and SAED pattern of our samples (Fig. 1(a) and Fig. 1(b)) give out that the crystal lattice *c* = 1.401 nm and *b* = 0.625 nm, which are the same as the reported WTe₂ single crystal structure [18,19]. Furthermore, the Energy Dispersive Spectrometer (EDS) experimental result confirms the stoichiometric WTe₂ (shown in the supplementary materials [20]).

An optical image of a typical WTe₂ single crystal for the transport measurement is shown in the inset of Fig. 1(c). The transport results reported here are primarily from Sample 1 with the size of $\sim 1.5 \text{ mm} \times 0.2 \text{ mm} \times 15 \text{ }\mu\text{m}$ (length \times width \times thickness). Standard four-electrode method was used for the measurements and the current is applied along the tungsten chains (*a* axis). Figure 1(c) shows the resistivity as a function of temperature at different magnetic fields, which are perpendicular to the chalcogenide layers (along the *c* axis). With decreasing temperature, the resistivity exhibits a well-metallic behavior at zero-field by showing a huge residual resistance ratio (RRR = 741), much larger than the reported values in other semimetals such as Bi [21] and NbSb₂ [22]. Interestingly, when applying the magnetic field, the resistivity displays a remarkable increase in low temperature regime showing a metal-insulator transition [23]. Figure 1(d) shows the Kohler's analysis of the resistivity curves at varies temperatures. According to Kohler's theory [24]:

$$\frac{\Delta\rho(T, \mu_0 H)}{\rho(T, 0)} = F\left(\frac{\mu_0 H}{\rho(T, 0)}\right), \quad (1)$$

where ρ is resistivity, T is temperature and H is magnetic field. If the carrier density of the system

is robust to temperature variation, the MR measured at different temperatures can be scaled into a single curve. Here, we assume the function $F\left(\frac{\mu_0 H}{\rho(T,0)}\right) = A(T)\left(\frac{\mu_0 H}{\rho(T,0)}\right)^2$ in the perpendicular field with parameter $A(T)$, due to the parabolic dependence of magnetic field at different temperatures when $H \parallel c$ axis. As shown in Fig. 1(d), the scaled MR curves deviate from the Kohler's rule with $A(T)$ changes with temperature, and the temperature effect is analyzed in the following part.

Figure 2 shows normalized MR ($\rho(H)/\rho(0)$) of WTe₂ measured in different field directions at varied temperatures. Schematic structure for the magnetotransport measurements is shown in Fig. 2(a). The current is applied along the a axis. In the perpendicular field ($H \parallel c$ axis) configuration, as shown in Fig. 2(b), pronounced Shubnikov-de Haas (SdH) oscillations are clearly visible around 5 T at 2 K. The MR reaches as high as 1,132,200% at 14.7 T and 2 K, about three times larger than the values reported before [11, 14]. With increasing temperature, MR decreases and the SdH oscillations are totally suppressed above 15 K. The field dependences of MR in the parallel field ($H \parallel b$ axis) at different temperatures are plotted in Fig. 2(c). The MR at low temperatures shows a classic parabolic dependence on the magnetic field with SdH oscillations at high fields. Compared to the MR measured in perpendicular field ($H \parallel c$ axis), the MR effect measured when $H \parallel b$ axis is decreased to $9 \times 10^4\%$ at 14.7 T at 2 K. Unexpectedly, when the magnetic field is parallel to the applied current along a axis, the MR shows a quite linear behavior rather than the parabolic behavior [Fig. 2(d)]. Even, the linear MR is as large as 1200% at $T = 2$ K and $\mu_0 H = 15$ T without any saturated trend. Moreover, the LMR property survives up to 50 K when the temperature is increased. Detailed analysis on the SdH oscillations is given in the supplementary materials [20].

To further investigate the Fermi surface of WTe₂, it is necessary to measure the angular-dependent MR behavior. Figure 3(a) shows MR behavior in a rotation by varying the relative magnetic field direction from c axis to b axis. The MR effect as well as the SdH oscillation is gradually weakened when rotating the magnetic field orientation away from c axis. Figure 3(b) demonstrates how the MR behavior changes in a rotation when the magnetic field is

varied from b axis ($H \perp I$) to a axis ($H \parallel I$). While MR is quadratically dependent on the magnetic field when $H \parallel b$ axis (0 deg), it deviates as H is rotated away from b axis. When $H \parallel I \parallel a$ axis, the MR exhibits a non-saturating but linear behavior, showing an extremely anisotropic characteristic of WTe_2 .

To understand better the angular-dependent MR in WTe_2 , we performed transport measurements to investigate the tilting-angle dependence of MR at 2 K at different magnetic fields [Fig. 3(c) and 3(d)]. As shown in Fig. 3(c), the observed angular dependence of MR in WTe_2 can be fitted by $|\cos\theta|$ function, where θ is the angle between magnetic field and c axis of WTe_2 . Moreover, when the magnetic field is tuned from b axis to a axis, the MR also shows obvious oscillations. These prominent MR oscillations with function form $|\cos\theta|$ indicates significant anisotropy of the carrier in the semimetal WTe_2 . Furthermore, the angular dependent MR oscillations are observed at high magnetic fields when the field rotating in the cb plane [Fig. 3(c)], which is absent in the rotation case in the ab plane [Fig. 3(d)]. When the magnetic field is lower than 6 T, the oscillations disappear, consistent with the observed SdH oscillations in WTe_2 .

To further reveal the anisotropic MR features in WTe_2 , we measured Sample 2 with the size of $\sim 1.2 \text{ mm} \times 0.29 \text{ mm} \times 25 \text{ }\mu\text{m}$ (length \times width \times thickness) from the same batch with current applied along the b axis ($I \parallel b$ axis). The MR properties of Sample 2 under different magnetic field directions are shown in Fig. 4(a)-(c). When the current is applied along b axis, the sample always displays classical quadratic MR for three different orientations of the magnetic field ($H \parallel c$ axis, $H \parallel b$ axis and $H \parallel a$ axis). The longitudinal LMR observed in Fig. 2(d) disappeared. It is believed that the LMR feature is related to the crystal direction, which needs further in-depth theoretical investigations. Additionally, as shown in Fig. 4(d), the angular dependent MR behavior also shows distinct MR oscillations with function form $|\cos\theta|$, similar to the behavior observed in Fig. 3(d), suggesting the anisotropy of the carrier in WTe_2 is independent of the applied current direction.

In order to confirm the exotic LMR in WTe_2 (when $H \parallel I \parallel a$ axis) is related to the crystal orientation, we also measured the MR behavior of Sample 2 when the current is applied along a axis. Temperature dependences of resistivity of Sample 2 for current along a and b axis are shown in Fig. 5(a). In high temperature region, the resistivity measured along b axis is about five times

higher than that measured along a axis. The low temperature regime is shown expanded in the inset. An obvious anisotropic behavior of resistivity can be observed in both high and low temperature region. Figure 5(b) displays the MR behavior in the perpendicular field ($H // c$ axis) when the current is parallel to the a axis. The MR effect is $1.1 \times 10^5 \%$ at 15 T at 2 K, which is about three times larger than the MR measured when $I // b$ axis [Fig. 4(a)], indicating an anisotropic MR behavior. In order to explore the exotic longitudinal LMR behavior, the detailed orientation dependent MR behavior around a axis is shown in Fig. 5(c). When the magnetic field is parallel to a axis, a perfect LMR is observed [inset of Fig. 5(c)], however, it changes to parabolic as H rotated away from a axis. The exotic LMR behavior may closely relate to the unique one dimensional tungsten chain (a axis). Nevertheless, further studies are needed to reveal the microscopic origin of the exotic LMR feature. Figure 5(d) displays the field dependent of MR at 2 K with the relative magnetic field rotating along from c axis (0 deg) to a axis (90 deg). It implies that the anisotropic behavior is general in WTe_2 system in regardless of the applied current direction.

In short, the transport property of WTe_2 system shows three distinct features: (i) the remarkable anisotropic resistivity and anisotropic MR when tuning the magnetic orientation; (ii) the violation of Kohler's law for MR behavior measured in the perpendicular field when $I // a$ axis; (iii) an exotic large LMR when the magnetic field parallel to the applied current direction along a axis.

Previously, it has been reported that WTe_2 possesses a large quadratic, non-saturating MR [11], due to the compensation of electron and hole carriers in the system [24]. Here, besides the non-saturating MR, we also observed profound anisotropic transport features. In specific, the anisotropic resistivity along a and b axis in Fig. 5(a) indicates that the effective mass of carrier satisfies $m_a \square m_b$. Moreover, as shown in Fig. 2(a) and (b), when $I // a$ axis, the MR measured when $H // c$ axis is an order of magnitude larger than that for $H // b$ axis, indicating the effective mass $m_b \square m_c$. These anisotropic effective mass of carrier can give rise to MR oscillations with function form $|\cos\theta|$ [shown in Fig. 3(c), 3(d), 4(d) and Fig. 5(d)]. Additionally, recent ARPES experiment demonstrates the complicated Fermi surface along $\Gamma - X$ lines [25], supporting the scenario of anisotropic mass of carrier in WTe_2 .

Next, we turn to the observed violation of Kohler's law for the MR measured in the

perpendicular field when $I // a$ axis. In the large field limit with $\mu(T)B \gg 1$, the MR can be written as [24]:

$$\frac{\Delta\rho(\mu_0 H, T)}{\rho_0(T)} = [\mu(T)\mu_0 H]^2 = \left[\frac{\mu_0 H}{n(T)e\rho_0(T)} \right]^2, \text{ with } \mu(T) \text{ and } n(T) \text{ denoting the mobility and}$$

total carrier density at temperature T . Commonly, the carrier density $n(T)$ is not sensitive to the change of temperature, which results in the Kohler's rule [24]. However, in WTe_2 with electron and hole carriers, the formation of excitons can change the carrier density, which leads to the violation of Kohler's rule similar to other correlated systems [26]. As shown in Fig. 1(d), the slope of scaling plot of MR firstly increases and then decreases around 20 K when increasing the temperature. This behavior indicates that the carrier density may also non-monotonically depend on the temperature—firstly decreasing then increasing. In WTe_2 single crystal, the electron and hole pockets lie separately along the $\Gamma-X$ line. The formation of excitons in three dimensional systems needs the perfect nesting of electron and hole pockets, which can hardly be satisfied due to different shapes of electron and hole Fermi surfaces. With increasing the temperature, the phonon with wave vector \vec{k}_0 and frequency $\omega(\vec{k}_0)$ appears, and connects the electron and hole pockets. This typical phonon mode can promote the formation of excitons, which leads to carrier density decreasing with increasing temperature. This formation of excitons is similar to the liquid-gas transition in previous studies [27, 28]. We find the phonon energy for $\omega(\vec{k}_0)$ lies in the range of 10 K~ 20 K (See the supplemental materials [20]). With increasing the temperature, thermal activation can destroy the excitons for temperature larger than the excitonic gap, resulting in the increase of carrier density for higher temperature. Overall, the phonons assist the exciton formation, and the thermal activation destructs the excitons. These double effects can give rise to the non-monotonic carrier density dependence on temperature and result in a minimum charge carrier density around 20 K.

Thirdly, we consider the origin of exotic large LMR when $H // I // a$ axis at low temperature. Classically, the resistance has no respond to the applied external magnetic field parallel to the excitation current. However, the quantum effect gives rise to Landau levels accompanied with quasi-1D dispersion along the magnetic field. In the quantum limit, the large degeneracy of

Landau levels leads to correlated effects. A well-known example is the charge density wave instability in Bismuth in the quantum limit [29, 30]. Specially in WTe_2 , the system has equal number of electron and hole carriers. The magnetic field $H // a$ axis leads to quasi-1D electron and hole states along $\Gamma-X$ line, and the density for each quasi-1D states satisfies $dN(n, k_x)/dk_x = eB/2\pi\hbar c$. The scattering between electron-like and hole-like Landau levels significantly increases with the increasing magnetic field, and contributes to the observed large LMR. Further study is expected to uncover the scattering and the exciton formation in this correlated compensate carrier system.

In summary, intriguing quantum transport properties of WTe_2 are revealed by systematic angle-dependent MR measurements at different temperatures. A large RRR in zero field and metal-insulator transition driven by perpendicular field are observed. More interestingly, the MR of WTe_2 shows extremely anisotropic properties. The parabolic MR reaches as high as 1.1322×10^6 % at 14.7 T at 2 K when $H // c$ axis but decreases to 9×10^4 % when $H // b$ axis. Surprisingly, an exotic large LMR as high as 1200% at 15 T is observed when $H // I // a$ axis. An empirical model of double carrier correlated system is developed based on the balanced hole-electron condition in WTe_2 to explain the observations. We expect that our research will encourage further theoretical and experimental studies on this exciting double carrier correlated layered material and corresponding new quantum properties.

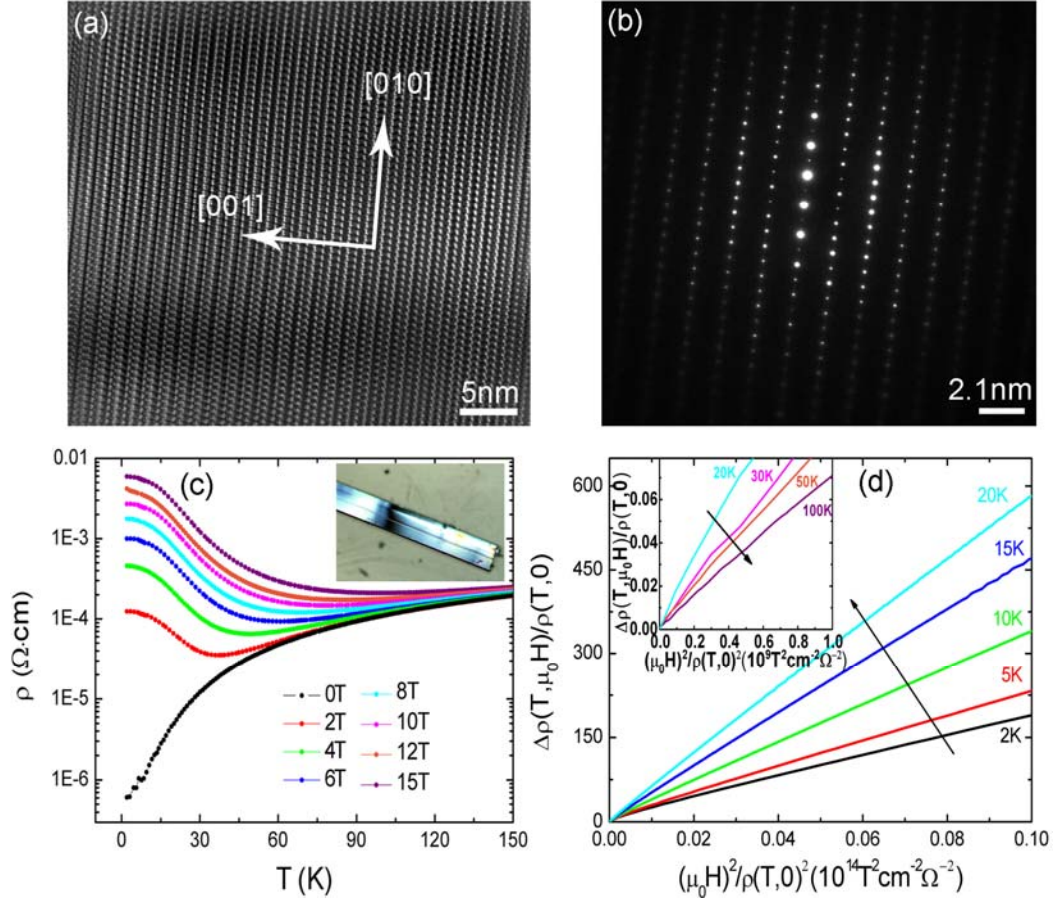


FIG 1. (color online). (a) High-resolution transmission electron microscopy image of WTe_2 single crystal. (b) Electron diffraction image looking down the $[100]$ zone axis showing the reciprocal lattice of WTe_2 . (c) Temperature dependence of longitudinal ρ of WTe_2 (Sample 1) at different magnetic fields. Inset: the optical image of WTe_2 single crystal. (d) Kohler's rule by plotting the $\rho(T, \mu_0 H)/\rho(T, 0)$ vs. $(\mu_0 H)^2/\rho(T, 0)^2$ from 2 K to 20 K. Inset show the high temperature regime from 20 K to 100 K.

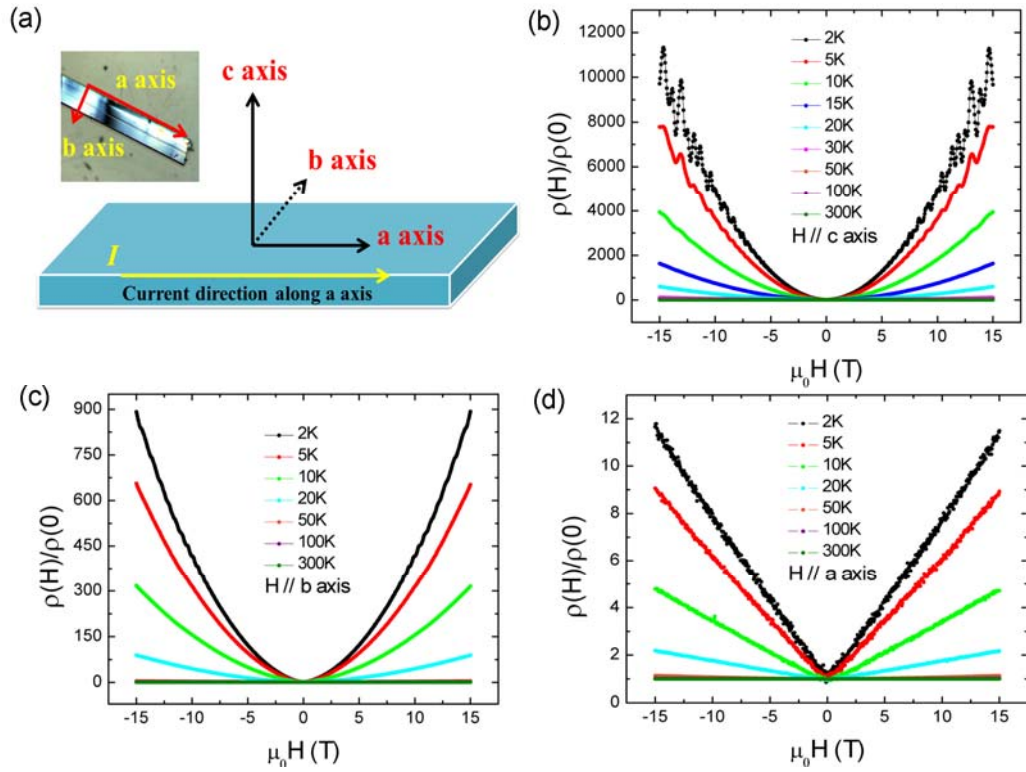


FIG 2. (color online). (a) Schematic structure for the magnetotransport measurements in WTe₂ system (Sample 1). Normalized magnetoresistivity $\rho(H)/\rho(0)$ of Sample 1 measured in (b) the perpendicular field ($H // c$ axis), (c) the parallel field with $H // b$ axis and (d) $H // a$ axis at different temperatures respectively.

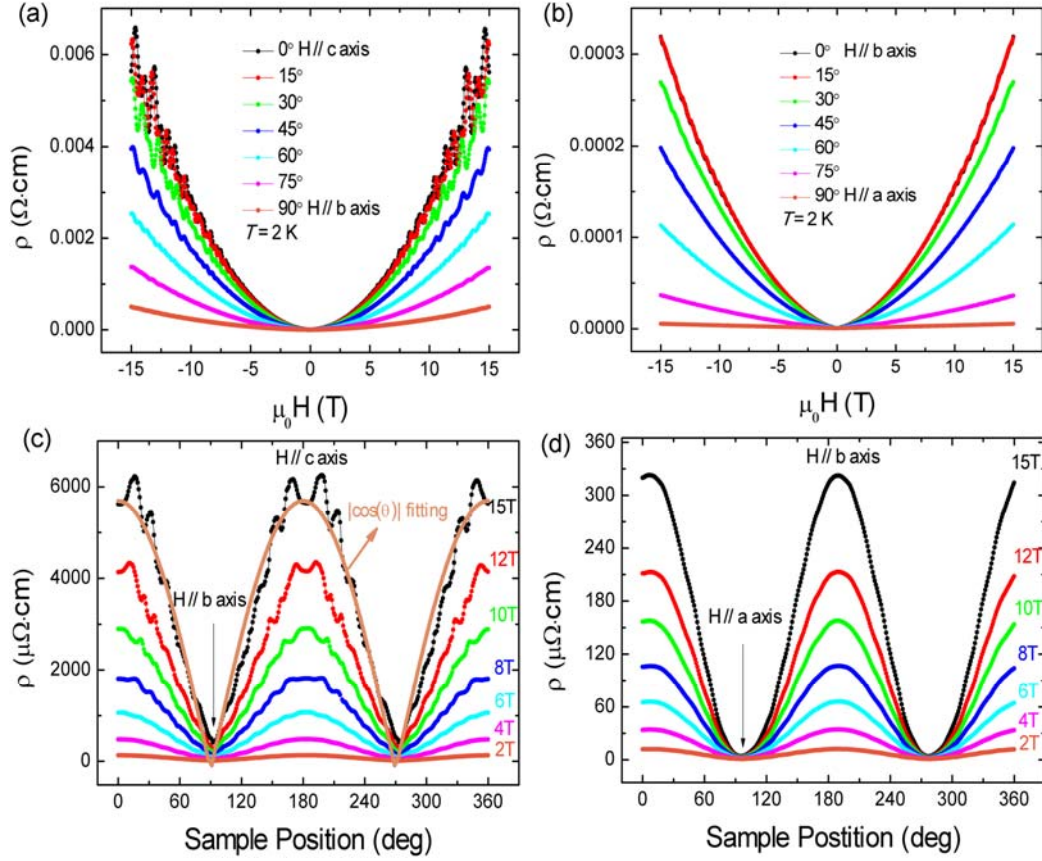


FIG 3. (color online). (a) Field dependent magnetoresistivity in Sample 1 at $T = 2$ K with the magnetic field rotating from c axis (0 deg) to b axis (90 deg) (b) Magnetoresistivity in Sample 1 measured at different angles in ab plane at $T = 2$ K (c) and (d) Magnetoresistivity in Sample 1 as a function of tilt angle in different magnetic fields at $T = 2$ K for the field rotating in the cb plane and ab plane, respectively. The function $|\cos\theta|$ fitting is shown as solid dark orange curve in Fig. 3(c).

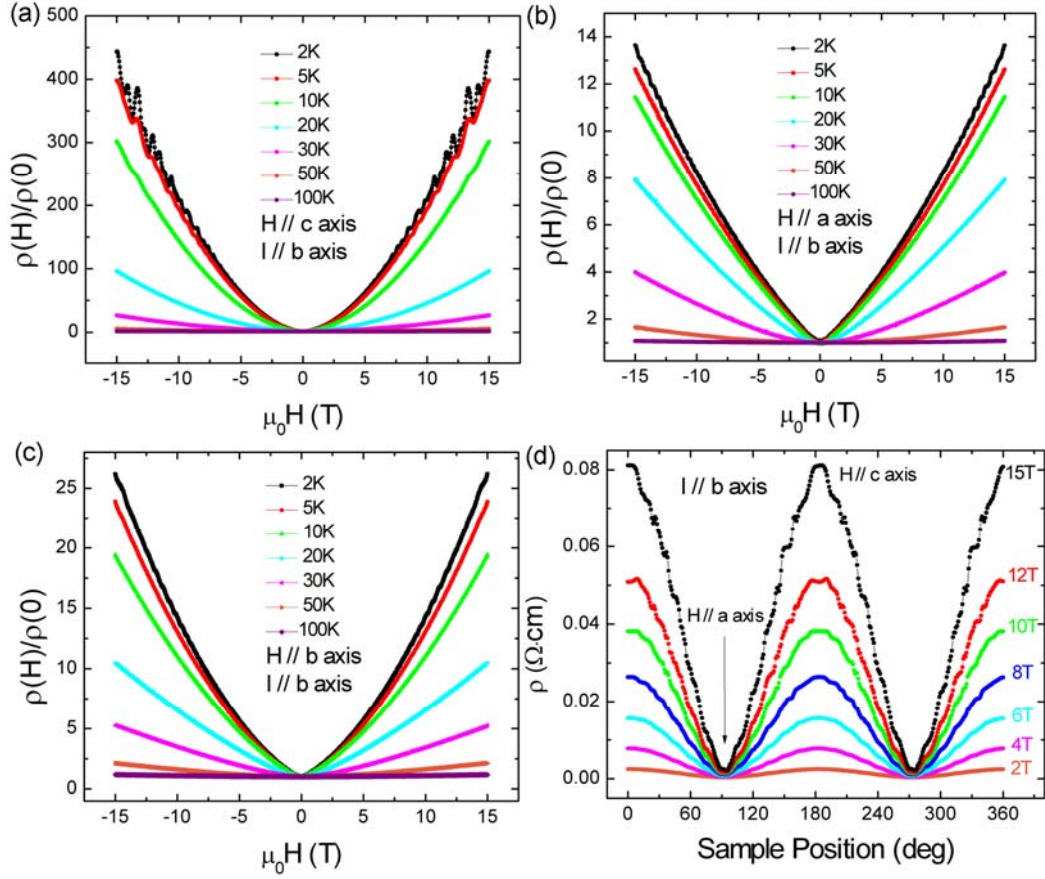


FIG 4. (color online). Normalized magnetoresistivity in Sample 2 with (a) the perpendicular field ($H // c$ axis), (b) the parallel field with $H // a$ axis and (c) $H // b$ axis at different temperatures, respectively. (d) Field dependent magnetoresistivity at $T = 2$ K with the magnetic field rotating from c axis (0 deg) to a axis (90 deg). The current is along the b axis.

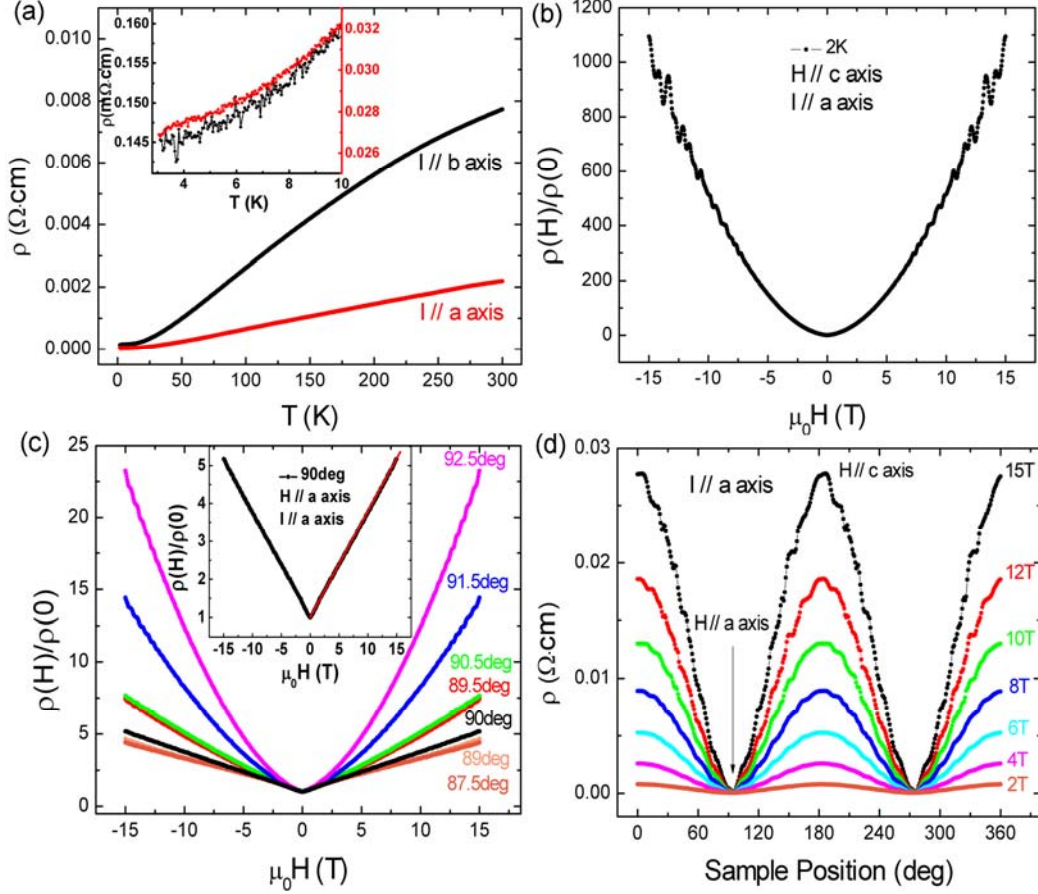


FIG 5. (color online). (a) Temperature dependence of resistivity in Sample 2 for current along a or b axis, respectively. Inset shows the expanded low temperature region. (b)-(c) show the normalized magnetoresistivity in Sample 2 for current along a axis in the perpendicular field ($H // c$ axis) or the parallel field with $H // a$ axis. Detailed orientation dependence is shown in (c) for H around a axis. Inset shows the LMR behavior when H is parallel to a axis. The red solid curve is linear fitting. (d) Field dependent magnetoresistivity at $T = 2$ K with the magnetic field rotating from c axis (0 deg) to a axis (90 deg). The current is along the a axis.

Acknowledgements

Yanfei Zhao and Haiwen Liu contributed equally to this work. We acknowledge Qian Niu, Fa Wang and Hua Chen for helpful discussions. This work was financially supported by National Basic Research Program of China (Grant Nos. 2013CB934600 and 2012CB921300), the National Natural Science Foundation of China (Nos. 11222434, 11174007), and the Research Fund for the Doctoral Program of

Higher Education (RFDP) of China. DGM acknowledges support from the Gordon and Betty Moore Foundation's EPIQS Initiative through Grant GBMF4416. JQY acknowledges support from the US Department of Energy, Office of Science, Basic Energy Sciences, Materials Sciences and Engineering Division. Y.W. acknowledges the support from Natural Science Foundation of China (11174244) and Zhejiang Provincial Natural Science Foundation of China (LR12A04002).

- [1] R. Xu, A. Husmann, T. F. Rosenbaum, M.-L. Saboungi, J. E. Enderby, and P. B. Littlewood, *Nature (London)* **390**, 57 (1997).
- [2] A. L. Friedman, J. L. Tedesco, P. M. Campbell, J. C. Culbertson, E. Aifer, F. K. Perkins, R. L. Myers-Ward, J. K. Hite, C. R. Eddy, Jr., G. G. Jernigan, and D. K. Gaskill, *Nano Lett.* **10**, 3962 (2010).
- [3] H. Tang, D. Liang, R. L. Qiu, and X. P. Gao, *Acs Nano* **5**, 7510 (2011).
- [4] X. Wang, Y. Du, S. Dou, and C. Zhang, *Phys. Rev. Lett.* **108**, 266806 (2012).
- [5] Y. Zhao, C.-Z. Chang, Y. Jiang, A. DaSilva, Y. Sun, H. Wang, Y. Xing, Y. Wang, K. He, X. Ma, Q.-K. Xue, and J. Wang, *Sci. Rep.* **3**, 3060 (2013).
- [6] L. Tian, Q. Gibson, M. N. Ali, M. Liu, R. J. Cava, and N. P. Ong, *Nat. Mater.* **14**, 280 (2014).
- [7] Y. Zhao, H. Liu, C. Zhang, H. Wang, J. Wang, Z. Lin, Y. Xing, H. Lu, J. Liu, Y. Wang, S. Jia, X. C. Xie, and J. Wang, arXiv: 1412.0330.
- [8] A. Narayanan, D. Watson, S. F. Blake, N. Bruyant, L. Drigo, Y. L. Chen, D. Prabhakaran, B. Yan, C. Felser, T. Kong, P. C. Canfield, and A. I. Coldea, *Phys. Rev. Lett.* **114**, 117201 (2015).
- [9] M. Novak, S. Sasaki, K. Segawa, and Y. Ando, arXiv: 1408.2183.
- [10] A. A. Abrikosov, *Phys. Rev. B* **58**, 2788 (1998).
- [11] M. N. Ali, J. Xiong, S. Flynn, J. Tao, Q. D. Gibson, L. M. Schoop, T. Liang, N. Haldolaarachchige, M. Hirschberger, N. P. Ong, and R. J. Cava, *Nature (London)* **514**, 205 (2014).
- [12] I. Pletikosić, M. N. Ali, A. V. Fedorov, R. J. Cava, and T. Valla, *Phys. Rev. Lett.* **113**, 216601 (2014).
- [13] H. Y. Lv, W. J. Lu, D. F. Shao, S. G. Tan, and Y. P. Sun, arXiv: 1412.8335.
- [14] P. L. Cai, L. P. He, J. Pan, X. C. Hong, Z. Zhang, J. Wei, Z. Q. Mao, and S. Y. Li, arXiv: 1412.8298.

- [15] X. C. Pan, X. Chen, H. Liu, Y. Feng, F. Song, X. Wan, Y. Zhou, Z. Chi, Z. Yang, B. Wang, Y. Zhang, and G. Wang, arXiv: 1501.07394.
- [16] D. Kang, Y. Zhou, W. Yi, C. Yang, J. Guo, Y. Shi, S. Zhang, Z. Wang, C. Zhang, S. Jiang, A. Li, K. Yang, Q. Wu, G. Zhang, L. Sun, and Z. Zhao, arXiv: 1502.00493.
- [17] X. Qian, J. Liu, L. Fu, and J. Li, *Science* **346**, 1344 (2014).
- [18] W. G. Dawson, and D. W. Bullett, *J. Phys. C: Solid State Phys.* **20**, 6159 (1987).
- [19] J. Augustin, V. Eyert, Th. Böker, W. Frentrup, H. Dwelk, C. Janowitz, and R. Manzke, *Phys. Rev. B* **62**, 812 (2000).
- [20] See supplementary materials.
- [21] P. L. Kapitza, *Proc. R. Soc. London Ser. A* **119**, 358 (1928).
- [22] K. Wang, D. Graf, L. Li, L. Wang, and C. Petrovic, *Sci. Rep.* **4**, 7328 (2014).
- [23] X. Du, S. -W. Tsai, D. L. Maslov, and A. F. Hebard, *Phys. Rev. Lett.* **94**, 166601 (2005).
- [24] J. M. Ziman, *Electrons and phonons: the theory of transport phenomena in solids*. Oxford, UK: Clarendon Press, (2001).
- [25] J. Jiang, F. Tang, X. C. Pan, H. M. Liu, X. H. Niu, Y. X. Wang, D. F. Xu, H. F. Yang, B. P. Xie, F. Q. Song, X. G. Wan, and D. L. Feng, arXiv: 1503.01422.
- [26] N. Luo, and G. H. Miley, *Physica C: Superconductivity* **371**, 259 (2002).
- [27] W. F. Brinkman, and T. M. Rice, *Phys. Rev. B* **7**, 1508 (1973).
- [28] S. He, and X. C. Xie, *Phys. Rev. Lett.* **80**, 3324 (1998); J. Shi and X. C. Xie, *Phys. Rev. Lett.* **88**, 086401 (2002).
- [29] D. Yoshioka and H. Fukuyama, *J. Phys. Soc. Jpn.* **50**, 725 (1981).
- [30] V. M. Yakovenko, *Phys. Rev. B* **47**, 8851 (1993).